

Research Article

Development of Polymeric Nanoparticles of *Garcinia mangostana* Xanthenes in Eudragit RL100/RS100 for Anti-Colon Cancer Drug Delivery

Abdalahim F. A. Aisha,¹ Amin Malik Shah Abdulmajid,¹ Zhari Ismail,² Salman A. Alrokayan,³ and Khalid M. Abu-Salah^{3,4}

¹Department of Pharmacology, School of Pharmaceutical Sciences, Universiti Sains Malaysia, 11800 Minden Barracks, Pulau Pinang, Malaysia

²Department of Pharmaceutical Chemistry, School of Pharmaceutical Sciences, Universiti Sains Malaysia, 11800 Minden Barracks, Pulau Pinang, Malaysia

³Chair of "Medical Applications of Nanomaterials", King Abdullah Institute for Nanotechnology, King Saud University, Riyadh 11451, Saudi Arabia

⁴Nanomedicine Section, King Abdullah International Medical Research Center, King Abdulaziz Medical City, Riyadh 11426, Saudi Arabia

Correspondence should be addressed to Amin Malik Shah Abdulmajid; aminmalikshah@gmail.com and Khalid M. Abu-Salah; abu-salahkh@ngha.med.sa

Received 25 May 2015; Revised 12 September 2015; Accepted 5 October 2015

Academic Editor: Ilaria Armentano

Copyright © 2015 Abdalahim F. A. Aisha et al. This is an open access article distributed under the Creative Commons Attribution License, which permits unrestricted use, distribution, and reproduction in any medium, provided the original work is properly cited.

Xanthenes are a group of oxygenated heterocyclic compounds with anticancer properties, but poor aqueous solubility and low oral bioavailability hinder their therapeutic application. This study sought to prepare a xanthenes extract (81% α -mangostin and 16% γ -mangostin) in polymeric nanoparticles and to investigate its intracellular delivery and cytotoxicity toward colon cancer cells. The nanoparticles were prepared in Eudragit RL100 and Eudragit RS100 by the nanoprecipitation method at drug loading and entrapment efficiency of 20% and >95%, respectively. Freeze-drying of bulk nanoparticle solutions, using glucose or sucrose as cryoprotectants, allowed the collection of nanoparticles at >95% yield. Solubility of the xanthenes extract was improved from 0.1 $\mu\text{g}/\text{mL}$ to 1250 $\mu\text{g}/\text{mL}$. Transmission electron microscopy (TEM) and dynamic light scattering (DLS) of the freeze-dried final formulation showed the presence of cationic round nanoparticles, with particle size in the range of 32–130 nm. Scanning electron microscopy (SEM) showed the presence of nanospheres, and Fourier transform infrared (FTIR) spectroscopy indicated intermolecular interaction of xanthenes with Eudragit polymers. Cellular uptake of nanoparticles was mediated via endocytosis and indicated intracellular delivery of xanthenes associated with potent cytotoxicity (median inhibitory concentration $26.3 \pm 0.22 \mu\text{g}/\text{mL}$). Presented results suggest that cationic nanoparticles of xanthenes may provide a novel oral drug delivery system for chemoprevention or treatment of intestinal and colon tumors.

1. Introduction

Xanthenes from *Garcinia mangostana* L. fruit rinds have been reported as potential anti-colon cancer candidates [1]. More than 50 xanthenes have been isolated from the fruit rind [2]; the most studied and abundant compounds are α -mangostin

(1,3,6-trihydroxy-7-methoxy-2,8-bis(3-methyl-2-butenyl)-9H-xanthen-9-one) and γ -mangostin (1,3,6,7-tetrahydroxy-2,8-bis(3-methylbut-2-enyl)xanthen-9-one) [2, 3] (Figure 1). The compounds are gaining remarkable interest due to their significant pharmacological effects such as anticancer [1, 4–7], anti-inflammatory [8, 9], antimicrobial [10, 11],

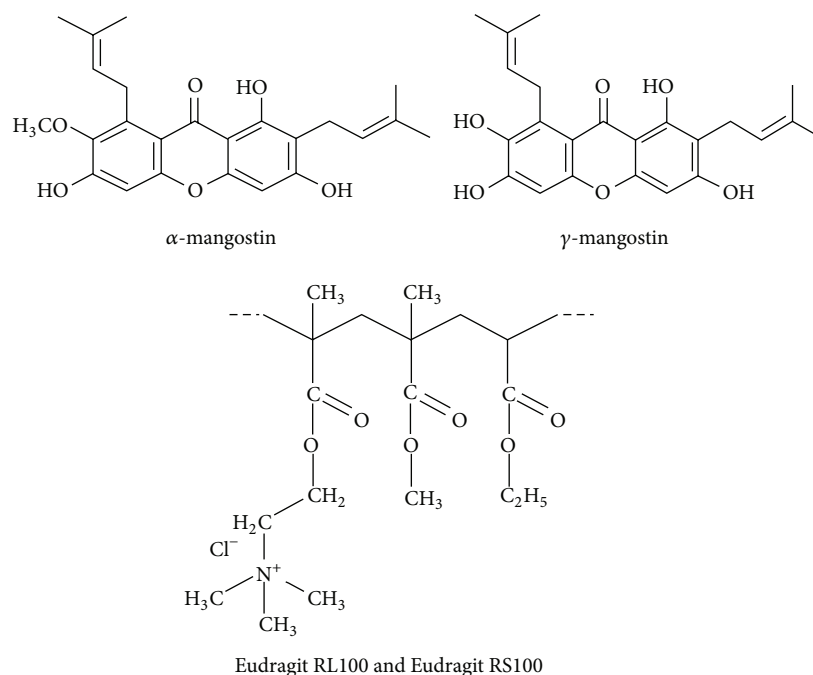


FIGURE 1: Chemical structure of α - and γ -mangostins (the main components of the xanthenes extract) and the Eudragit RL100 and Eudragit RS100 polymers.

cardioprotective [12], analgesic [13], and antioxidant effects [14], as well as enhancement of the immune system [15, 16].

In a previous study conducted in our lab, a xanthenes extract prepared from *G. mangostana* fruit rinds showed potent *in vitro* anti-colon cancer activity equivalent to that of pure α -mangostin. The anticancer effect of the extract was mediated via upregulation of the p53, Myc/Max, and MAPK/ERK cell signaling pathways [17]. Therefore, this extract (containing 81% α -mangostin and 16% γ -mangostin) may provide a cost-effective alternative to the pure compound in the treatment or chemoprevention of colon cancer. However, the extract and α -mangostin suffer poor aqueous solubility and very low oral bioavailability [18]; these can be major obstacles toward the therapeutic application of *G. mangostana* xanthenes.

Polymeric nanoparticles are versatile drug delivery systems that can improve aqueous solubility and overcome the physiologic barriers to deliver drugs to their site of action. This study utilized the time-dependent colon targeting approach by using the cationic polymers Eudragit RL100 (E-RL100) and Eudragit RS100 (E-RS100). These are copolymers of ethyl acrylate, methyl methacrylate, and a low content of a methacrylic acid ester with quaternary ammonium groups (Figure 1). The ammonium groups are present as salts and make the polymers permeable.

Due to their low chemical reactivity and low toxicity, these polymers have been widely used in tablet coating to provide time-dependent colonic targeting and recently reported in preparation of mucoadhesive and time-dependent release nanoparticles (NPs) [19]. Their cationic charge and mucoadhesive properties [20, 21] provide direct contact of the NPs

with the gastrointestinal tract (GIT) mucosa, which may increase the likelihood of cellular uptake by endocytosis and increase the transit time of NPs in the GIT, leading to improved therapeutic efficacy. The endocytotic uptake of NPs has been extensively reported as a novel approach to overcome multidrug resistance, the major cause of drug failure in cancer chemotherapy [22]. This study reports preparation, characterization, and intracellular delivery of cationic NPs of *G. mangostana* xanthenes in E-RL100/E-RS100 polymers, as a time-dependent and intracellular drug delivery system.

The NPs were prepared by nanoprecipitation at various drug loading, polymer concentration, E-RL100 : E-RS100 ratio, and surfactants. The NPs were collected by freeze-drying of the bulk NP solutions, the drug content was determined by UV spectrophotometry, and the particle size and zeta potential were determined by dynamic light scattering (DLS). NPs morphology was studied by TEM and SEM, the interaction between the polymers and the extract was investigated by FTIR, and the intracellular delivery of NPs was investigated on human colorectal carcinoma cell line HCT 116 by fluorescent microscopy.

2. Materials and Methods

2.1. Materials. E-RS100 and E-RL100 were obtained as a gift from Evonik Degussa (International Business Park, Nordic European Centre, Singapore). The reference compounds were purchased from ChromaDex (Irvine, California). Penicillin/streptomycin solution, dimethyl sulfoxide (DMSO), phosphate buffered saline (PBS), tween 80, tween 20, polyvinyl alcohol-72000 Dalton (PVA-72000 Da), glucose, glycine,

sucrose, dextran 40000 Da, glycerol, mannitol, 2,3-bis(2-methoxy-4-nitro-5-sulfophenyl)-2h-tetrazolium-5-carboxanilide inner salt (XTT), and phenazine methosulfate (PMS) were purchased from Sigma-Aldrich (Kuala Lumpur, Malaysia). Analytical grade acetone and high-performance liquid chromatography (HPLC) grade acetonitrile were obtained from Avantor Performance Materials (Petaling Jaya, Selangor, Malaysia). HCT 116 cell line was purchased from the American Type Culture Collection (ATCC, Manassas, Virginia). RPMI 1640 cell culture medium (without phenol red) and fetal bovine serum (FBS) were purchased from Bio-Diagnostics (Petaling Jaya, Selangor, Malaysia).

2.2. Preparation and Standardization of the Xanthonex Extract. The xanthonex extract was obtained at 5% yield (wt/wt) from *G. mangostana* fruit rinds and was standardized by Liquid Chromatography-Mass Spectrometry (LC-MS) [17]. Briefly, the fruit rind powder was macerated in toluene at 60°C for 48 h, filtered, concentrated, and crystallized at 2–8°C for 24 h to give a yellow precipitate. The precipitate was collected and further dried at 50°C for 24 h.

The concentration of total xanthonex was determined by Ultraviolet (UV) spectrophotometry. In brief, the optical density (OD) of a methanolic solution of the extract (50 µg/mL) was measured at 243.4 nm, and the concentration of total xanthonex was then determined by applying the linear regression equation of α -mangostin reference compound. The result is presented as % (wt/wt) as the following:

$$\begin{aligned} \text{Total xanthonex \% (wt/wt)} \\ = \left(\frac{\text{Calculated xanthonex concentration}}{\text{Theoretical xanthonex concentration}} \right) \times 100. \end{aligned} \quad (1)$$

Dionex-Ultimate 3000 HPLC system, coupled with a Micro TOF-Q mass spectrometer, was used in the MS analysis of the extract. Separation was carried out on a reverse phase Nucleosil C18 column (5 µm, 4.6 × 250 mm) at 30°C with a mobile phase consisting of 95% acetonitrile and 5% of 0.1% H₃PO₄ in water, for 10 min at 0.5 mL/min. The spectral data were collected at 244 nm, and mass scanning was set in the range of 50–1000 *m/z*, in the negative ion mode with the nebulizer set to 3.0 bars and heated to 150°C. The capillary voltage was set at 3000 V using a nitrogen dry gas at a flow rate of 8.0 L/min. The end plate offset was maintained at –500 V.

2.3. Determination of Aqueous Solubility of the Xanthonex Extract. Aqueous solubility of the xanthonex extract was determined by the shake flask method [23]. The experiment was carried out at 37°C in PBS at pH 7.4, with various concentrations (wt/v) of tween 80 (0.0, 0.1, 0.5, 1.0, and 2.0%). Briefly, 5 mg of pulverized extract was added to 25 mL glass vials containing 10 mL buffered solutions. The samples were then mixed for 24 h in a shaker incubator at 200 rpm. Subsequently, the samples were filtered through 0.2 µm syringe filters, and the concentration of total xanthonex was determined by UV spectrophotometry as mentioned above.

2.4. Preparation of the NPs. NPs of the xanthonex extract were prepared in E-RL100 and E-RS100 by the nanoprecipitation

method developed by Fessi et al. [24]. The polymers and the extract were dissolved separately in acetone at room temperature (RT). The organic phase was then prepared by mixing both solutions on a magnetic stirrer for 30 min. Subsequently, the organic phase was added slowly to the aqueous phase (double distilled water (dd.H₂O) with or without surfactants) by means of syringe attached to a 27 G needle, inserted directly into the aqueous phase while mixing at 700 rpm. Acetone was then evaporated at 50°C on a magnetic stirrer at 600 rpm for 4 h, and the agglomeration (if any) was removed by vacuum-filtration through a 0.8 µm membrane filter.

2.5. Determination of the Entrapment Efficiency. The solvent was removed as described above and the precipitated free drug and the agglomerated NPs (if any) were removed by vacuum-filtration through a 0.8 µm membrane filter giving transparent NP solutions. The entrapment efficiency was then determined by UV spectrophotometry as the following: the transparent NP solutions were diluted in methanol, and the OD was recorded at 243.4 nm. The xanthonex concentration was determined as mentioned above, and the entrapment efficiency was then calculated by applying the following formula:

$$\begin{aligned} \% \text{ Entrapment efficiency} \\ = \left(\frac{\text{Measured xanthonex concentration}}{\text{Theoretical xanthonex concentration}} \right) \times 100. \end{aligned} \quad (2)$$

2.6. Freeze-Drying of Bulk NPs Solutions. The effect of various surfactants and cryoprotectants was evaluated on the freeze-drying process. Ten milliliters of the bulk NP solutions was frozen in 25 mL glass vials, with or without cryoprotectants, at –18°C for 12 h. The solid solutions were then freeze-dried under vacuum at –50°C for 48 h using Labconco FreeZone 6 drying system (Labconco, Kansas City, Missouri) and further dried at 50°C for 5 h.

2.7. Evaluation of Freeze-Drying Efficiency. The efficiency of freeze-drying process was determined by studying the cake morphology, the ease of reconstitution, and aqueous solubility of the freeze-dried NPs.

The freeze-dried cakes were identified as intact with the same volume (IS), collapsed (C), or partially collapsed (PC).

The freeze-dried cakes were then reconstituted in the same volume of water and were given a score as the following: reconstituted immediately (++++), reconstituted after several manual inversions for 1 min (+++), reconstituted after vortex for 1 min (++) , reconstituted after sonication (+), and not reconstituted after sonication (0) [25].

Concentration of the soluble fraction of the entrapped xanthonex (aqueous solubility) in the reconstituted NPs was determined as the following: the reconstituted NP solutions were centrifuged at 2300 ×g for 5 min using Tomy MX-305 centrifuge (Tomy Seiko Co. Ltd., Tokyo, Japan), the supernatant was filtered through a 0.2 µm syringe filter, and the concentration of total xanthonex in the filtrate was measured by UV spectrophotometry as mentioned in the previous sections.

2.8. Determination of the Percentage Yield. The bulk NPs solutions were freeze-dried as mentioned above. The vials were weighed accurately, and the weight of NPs was determined from the difference between the empty and loaded vials. The percentage yield was then calculated using the following formula:

$$\% \text{ Yield} = \left(\frac{W_R}{W_T} \right) \times 100, \quad (3)$$

where W_R is the recorded weight of freeze-dried NPs and W_T is the theoretical yield of polymers, drug, and surfactant.

2.9. Measurement of the Particle Size and Zeta Potential. Particle size, polydispersity index (PDI), and zeta potential (ζ) were determined by DSL using a Zetasizer nano zs (Malvern Instruments Ltd., Malvern, Worcestershire, UK). The samples were filtered through a 0.2 μm syringe filter, and the measurements were carried out in triplicate.

To examine the effect of pH on particle size and zeta potential, the freeze-dried formulation was reconstituted in dd.water and then diluted in phosphate buffered saline (PBS) at various pH values (5.5, 6.8, and 7.4); the samples were mixed well and incubated in a water bath at 37°C for 18 hours. The agglomeration (if any) was removed by filtration through a membrane filter (0.8 μm).

2.10. Transmission and Scanning Electron Microscopy. One drop of the NP solution was deposited on a 400-mesh copper grid coated with 5 nm layer of carbon and air-dried at RT. The samples were then studied at different magnifications in a Philips CM12 TEM used to study the samples. Morphology and dispersity of freeze-dried NPs were examined by SEM. The samples were freeze-dried, with or without cryoprotectant, coated with 3–6 nm Platinum by sputter deposition at –120°C, and analyzed in a LEO Supra 50 VP field emission of Carl Zeiss SEM.

2.11. Fourier Transform Infrared Spectroscopy. The interaction between the E-RL100/E-RS100 and the xanthenes extract was investigated using attenuated total reflectance FTIR (ATR/FTIR) spectroscopy as measured with a Perkin Elmer Spectrum 400 spectrometer. The spectra of nonformulated xanthenes, empty NPs, physical mixtures (PMs), and loaded NPs were recorded in the range of 4000–650 cm^{-1} ($n = 3$). To ensure the homogenous PMs formation, the components were ground to a fine powder and thoroughly mixed using a mortar and pestle.

2.12. Evaluation of the In Vitro Release. *In vitro* release studies were performed under sink conditions (1:12) by reverse dialysis method at 37°C with continuous stirring at 100 rpm. Five milliliters of NPs solution (equivalent to 6.2 mg of xanthenes extract) was diluted in 500 mL release medium (0.5% tween 80 in PBS). Sixteen dialysis bags (molecular weight cut-off 8200 Da) were loaded with 2 mL release medium, hermetically sealed, and kept in the donor compartment. The drug release was studied at different pH values in sequence, namely, 1.6 (2 h), 5.5 (1 h), 6.8 (3 h), and 7.5 (42 h) [26]; the pH

was adjusted by adding 5 M NaOH. One bag was removed at 0, 0.5, 1, 2, 3, 4, 5, 6, 9, 12, 18, 24, 30, 36, 42, and 48 h. The bag content was filtered through a 0.45- μm syringe filter and was analyzed by HPLC as follows: Dionex-Ultimate 3000 HPLC system (Dionex, Sunnyvale, California) was used. Separation was carried out on a reverse phase Nucleosil C18 column (5 μm , 4.6 \times 250 mm) (Macherey Nagel, Bethlehem, Pennsylvania) at 30°C with a mobile phase consisting of 95% acetonitrile and 5% of 0.1% H_3PO_4 in water, for 10 min at 1.0 mL/min. The spectral data were collected at 244 nm. The experiment was repeated 3 times and the results are presented as average percentage of cumulative release \pm SD.

2.13. Evaluation of the Intracellular Delivery of NPs. The intracellular delivery of NPs was investigated on HCT 116 cell line as an *in vitro* model of human colorectal carcinoma [27], as previously described [28]. Cells were maintained in RPMI 1640 culture medium (without phenol red) and supplemented with 10% FBS and 1% penicillin/streptomycin. Seventy to eighty percent of confluent cultures were treated with the NPs at 20 $\mu\text{g}/\text{mL}$ for 6 h. Subsequently, the cells were washed extensively with PBS, fixed in 4% paraformaldehyde, and visualized immediately at 96x magnification of Olympus IX71 inverted fluorescent microscope (Olympus, Shinjuku, Tokyo, Japan), using the blue filter and maintaining all settings constant for all treatments.

2.14. Evaluation of Cytotoxic Effect. Cytotoxicity of the non-formulated xanthenes extract, loaded and empty NPs, was evaluated on HCT 116 cells using XTT assay as previously described [29]. Cells were seeded in 96-well plate at 1×10^4 /well in 100 μL of medium. After overnight incubation, further 100 μL of fresh medium containing the treatment compounds was added and incubated for 48 h. Cell viability was then determined as follows: 20 μL of a mixture of XTT (1 mg/mL) and PMS (10 $\mu\text{g}/\text{mL}$) was added and incubated for 4 h. Later, OD was measured at 450 nm using Thermo Fisher Scientific microplate reader. Cell-free medium was used as a blank, and cells treated with the vehicle alone (0.5% DMSO) were used as negative control, and both were processed in the same manner as the treated cells. Percentage inhibition was then calculated using the following formula:

$$\% \text{ inhibition} = \left(1 - \frac{(\text{OD}_{\text{samples}} - \text{OD}_{\text{blank}})}{(\text{OD}_{\text{control}} - \text{OD}_{\text{blank}})} \right) \times 100. \quad (4)$$

The results are presented as average \pm SD ($n = 4$), and the median inhibitory concentration (IC_{50}) was calculated from the dose response curves.

2.15. Statistical Analysis. Results are presented as average \pm SD. Statistical analysis was carried out by one-way ANOVA using SSPS software package 16.0, and difference between groups was considered significant at $P < 0.05$.

3. Results and Discussion

3.1. Standardization of the Xanthenes Extract. Three batches of the xanthenes extract were analyzed by UV spectrophotometry and LC-MS. UV λ_{max} was 243.4 nm, and the average

TABLE 1: Effect of 3 levels of the polymer and drug loading on particle size. Nine NP formulations were prepared at 3 levels of drug loading and polymer concentration using acetone as the solvent and water without surfactants as antisolvent. The solvent was evaporated and the particle size was measured by dynamic light scattering. The results are presented as average particle size \pm SD ($n = 3$).

Formulation	Polymer conc. (mg/mL)	Drug loading % (wt/wt)	Particle size \pm SD (nm)	Polydispersity index
F1	25	20	32.0 \pm 2.4	0.53
F2	25	33	39.0 \pm 0.5	0.43
F3	25	43	52.0 \pm 0.4	0.34
F4	50	20	44.0 \pm 1.4	0.38
F5	50	33	58.0 \pm 0.6	0.32
F6	50	43	70.0 \pm 0.6	0.40
F7	100	20	72.0 \pm 0.5	0.26
F8	100	33	70.0 \pm 0.2	0.32
F9	100	43	70.0 \pm 0.4	0.34

xanthonones concentration was $98.6 \pm 1.3\%$ (wt/wt). LC-MS analysis showed the presence of 5 compounds: α -mangostin ($80.8 \pm 1.6\%$), γ -mangostin ($15.6 \pm 1.6\%$), garcinone c ($1.4 \pm 0.1\%$), 8-deoxygartanin ($1.2 \pm 0.1\%$), and β -mangostin ($0.9 \pm 0.03\%$). The results indicate good reproducibility of extraction and standardization procedures.

3.2. Aqueous Solubility of the Xanthonones Extract. In the absence of tween 80, the aqueous solubility of the extract was $0.1 \pm 0.01 \mu\text{g/mL}$, which was improved to 37.0 ± 0.5 , 150.0 ± 0.6 , 263.0 ± 2.0 , and $409.0 \pm 3.0 \mu\text{g/mL}$, by adding tween 80 at 0.1, 0.5, 1.0, and 2.0% (wt/v), respectively.

3.3. Effect of Polymer Concentration and Drug Loading on Particle Size. The polymer was made of 1:1 mixture (wt/wt) of E-RL100 : E-RS100, the aqueous phase was dd.H₂O without surfactant, and the effect of 3 levels of the polymer and drug loading was investigated on particle size. The results indicate spontaneous formation of NPs upon addition of the drug/polymer solution to the aqueous phase. At 25 and 50 mg/mL of the polymer, the particle size was increased, in a dose-dependent manner, by increasing the drug loading (Table 1). However, at 100 mg/mL of the polymer, changing the drug loading has no significant effect on particle size ($P > 0.05$), though the particle size was higher than that at 25 and 50 mg/mL. The data also indicate the presence of surfactants is not essential for the formation of NPs in this method, which was also reported by other researchers [30, 31]. After a storage for few days at RT, crystal growth was noticed in formulations prepared at 33% and 43% drug loading and those prepared at 100 mg/mL of the polymer, which indicates instability of the NPs. Therefore, polymer concentration at 50 mg/mL and drug loading at 20% were selected for further optimization of the production of NPs.

3.4. Optimization of E-RL100 : E-RS100 Ratio. Polymer concentration was fixed at 50 mg/mL, the drug loading was set at 20%, and the aqueous phase was dd.H₂O without surfactant. The effect of various E-RL100 : E-RS100 ratios was investigated on the entrapment efficiency, particle size, PDI, zeta potential, and the percentage yield (Table 2). There was no significant effect of the ratio of the two polymers on the entrapment efficiency ($P = 0.37$). On the other hand, the particle size, zeta potential, and the percentage yield were significantly affected, with P values < 0.05 . Furthermore, the particle size was substantially decreased by increasing the E-RL100 : E-RS100 ratio by $\geq 3:1$.

The NPs bulk solutions were then freeze-dried with 1% sucrose as cryoprotectant and were reconstituted in the same volume of dd.H₂O. The aqueous solubility and particle size were significantly affected by changing the ratio of the two polymers ($P = 0.0$) (Table 3). The highest aqueous solubility and smallest NPs were obtained at 3:1 ratio E-RL100 : E-RS100. Therefore, this ratio was selected for further optimization in the production of NPs of the xanthonones extract.

3.5. Effect of pH on Particle Size and Zeta Potential. The particle size and the zeta potential of nanoparticles in the freeze-dried final formulation were found to increase upon decreasing the pH of the medium due to increased hydronium ions concentrations which is accompanied by a decrease in the polydispersity index (Table 4).

3.6. Effect of Surfactants on Particle Size and Entrapment Efficiency. In this study, the polymer concentration was set at 50 mg/mL at 3:1 ratio E-RL100 : E-RS100 and 20% drug loading. The effect of 2 levels of 3 surfactants was investigated on particle size and entrapment efficiency. The results showed that entrapment efficiency was not affected by the presence of the surfactants, and it was 100% in all formulations. On the other hand, the surfactants have significant effect on the particle size ($P = 0.0$), where the smallest NPs were obtained at 0.1% tween 80 and 0.05% tween 20 (Table 5). It might be assumed that the high entrapment efficiency is due to the presence of free compounds in the NPs solution. This presumption was excluded as follows: the free xanthonones showed low aqueous solubility ($37.0 \pm 0.5 \mu\text{g/mL}$) at tween 80 concentration of 0.1%. In the NPs solution, at the same tween 80 concentration, the concentration of soluble xanthonones was found to be $1250.0 \pm 4.0 \mu\text{g/mL}$. If there are untrapped xanthonones in the NPs solution, their concentration should not exceed $37.0 \pm 0.5 \mu\text{g/mL}$, and any xanthonones beyond this concentration tend to precipitate and can be removed by filtration. Therefore, we can conclude that the high entrapment efficiency of xanthonones in the Eudragit NPs is not due to the presence of free xanthonones in the solution, but due to entrapment of xanthonones in the NPs leading to substantial improvement in their aqueous solubility.

3.7. Optimization of Freeze-Drying Process. The NPs in this study were produced at polymer concentration of 50 mg/mL, 3:1 E-RL100 : E-RS100, 20% drug loading, and with or without surfactants. The bulk NP solutions of 7 formulations

TABLE 2: Effect of the E-RL100 : E-RS100 ratio on NPs characteristics. NPs were prepared without surfactants at 20% drug loading and various E-RL100 : E-RS100 ratios. The solvent was evaporated, the free drug was removed by filtration, and the entrapment efficiency, particle size, polydispersity index, zeta potential, and percentage yield were determined. The results are depicted as average \pm SD ($n = 3$).

Formulation	E-RL100 : E-RS100 (wt/wt)	E. efficiency (%)	P. size (nm)	Polydispersity index	Z. potential (mV)	Yield (%)
F1	0 : 1	96.0 \pm 7.0	72.0 \pm 0.4	0.21 \pm 0.01	34.0 \pm 0.7	86 \pm 0.1
F2	1 : 3	96.0 \pm 6.0	77.0 \pm 0.6	0.19 \pm 0.01	32.0 \pm 0.9	92 \pm 0.1
F3	1 : 1	101.0 \pm 1.0	65.0 \pm 0.4	0.20 \pm 0.00	34.0 \pm 2.9	98 \pm 0.2
F4	3 : 1	94.0 \pm 0.1	45.0 \pm 0.3	0.19 \pm 0.01	31.0 \pm 1.0	99 \pm 0.3
F5	1 : 0	98.0 \pm 1.0	46.0 \pm 0.1	0.21 \pm 0.00	30.0 \pm 1.4	91 \pm 0.3

TABLE 3: Effect of E-RL100 : E-RS100 ratio on the aqueous solubility and particle size of freeze-dried NPs. The NPs (20% drug loading) bulk solutions were freeze-dried with 1% (wt/v) sucrose and the resulting cakes were reconstituted in the same volume of water, vortexed for 1 min, and sonicated for 10 min, and the insoluble material was removed by centrifugation. The drug content in the supernatant was measured by UV spectrophotometry and the particle size was measured by photon correlation spectroscopy. The results are presented as average solubility ($\mu\text{g/mL}$) and average particle size (nm) ($n = 3$).

Formulation	E-RL100 : E-RS100 (wt/wt)	Aqueous solubility ($\mu\text{g/mL}$)	Particle size (nm)	Polydispersity index
F1	0 : 1	340.0 \pm 3.0	130.0 \pm 0.2	0.43 \pm 0.12
F2	1 : 3	917.0 \pm 22.0	83.0 \pm 0.7	0.21 \pm 0.01
F3	1 : 1	972.0 \pm 12.0	72.0 \pm 0.4	0.25 \pm 0.01
F4	3 : 1	968.0 \pm 2.0	52.0 \pm 0.2	0.24 \pm 0.00
F5	1 : 0	591.0 \pm 6.0	84.0 \pm 0.5	0.20 \pm 0.01

TABLE 4: Effect of pH on particle size and zeta potential. The freeze-dried final formulation was reconstituted in dd.water and then diluted in phosphate buffered saline at various pH values (5.5, 6.8, and 7.4); the samples were mixed well and incubated in water bath at 37°C for 18 h. The agglomeration (if any) was removed by filtration through membrane filter (0.8 μm). The results are presented as average \pm SD ($n = 3$).

pH	Size (nm)	Zeta potential (mV)	PDI
7.4	42.0 \pm 0.3	0.8 \pm 2.2	0.60 \pm 0.01
6.8	73.0 \pm 0.6	3.0 \pm 2.1	0.30 \pm 0.01
5.5	85.0 \pm 0.4	4.2 \pm 0.4	0.17 \pm 0.01

were freeze-dried with 6 cryoprotectants, and a formulation was freeze-dried without a cryoprotectant for reference. The cryoprotectants were used at a final concentration of 0.25% (wt/v), and the cryoprotectant(s) with the highest cryopreservation effect was selected based on the cake appearance, ease of reconstitution, and xanthonic aqueous solubility.

Based on the cake appearance, the freeze-dried NPs were classified into 3 categories: intact with same volume (IS), partially collapsed (PC), or collapsed (C) (Table 6).

The freeze-dried NPs were then reconstituted in the same volume of dd.water and were given a score as described in the materials and methods. The results are displayed in Table 7.

The aqueous solubility of freeze-dried NPs was then utilized in the selection of cryoprotectants. The highest

solubility was achieved in NPs freeze-dried with glycerol, glucose, and sucrose, particularly in the formulation prepared with 0.1% tween 80 (Table 8). Mannitol, glycine, and dextran produced intact cakes, but with low aqueous solubility, which suggests them to be bulking reagents. The results also indicate that freeze-drying without a cryoprotectant resulted in irreversible agglomeration of the NPs leading to very low reconstitution. Though the presence of surfactants is not essential for the formation of NPs in this method, the NPs prepared without surfactants showed very low reconstitution compared to those prepared with 0.1% tween 80, which indicates the crucial role of tween 80 in the success of the freeze-drying process.

3.8. Optimization of Glucose, Sucrose, and Glycerol Concentration. The NPs prepared with 0.1% tween 80 were chosen, and the aqueous solubility was selected as the marker for optimizing the cryoprotectant concentration. Glucose, glycerol, and sucrose were used in the concentration range of 0.125–1.0% (wt/v). The results showed a dose response effect on aqueous solubility and hence on reconstitution of freeze-dried NPs (Table 9). The freeze-dried formulation prepared with glycerol produced collapsed cakes but totally reconstituted after sonication. On the other hand, intact cakes were obtained in both glucose and sucrose, and the NPs were reconstituted either immediately (++++) or after several manual inversions (+++). The formulation with successful freeze-drying produced clear solutions after reconstitution in water, whereas those that made the freeze-drying process fail did not redisperse and showed obvious agglomeration of NPs (Figure 2). Collectively, the best freeze-drying results were

TABLE 5: Effect of surfactants on entrapment efficiency and particle size. The NPs were prepared at 20% drug loading with various surfactants, and the entrapment efficiency and particle size were measured by UV spectrophotometry and photon correlation spectroscopy, respectively. The results are presented as average \pm SD ($n = 3$).

Formulation	Surfactant	Surfactant conc. % (wt/v)	Entrapment efficiency (%)	Particle size (nm)	Polydispersity index
F4-A	Tween 80	0.10	100.0 \pm 0.3	39.0 \pm 0.1	0.24 \pm 0.01
F4-B	Tween 80	0.05	100.0 \pm 0.3	48.0 \pm 0.2	0.20 \pm 0.01
F4-C	Tween 20	0.10	100.0 \pm 0.5	44.0 \pm 0.1	0.22 \pm 0.01
F4-D	Tween 20	0.05	100.0 \pm 0.7	39.0 \pm 0.1	0.20 \pm 0.01
F4-E	PVA	0.10	100.0 \pm 0.4	55.0 \pm 0.2	0.21 \pm 0.01
F4-F	PVA	0.05	100.0 \pm 0.3	47.0 \pm 0.1	0.21 \pm 0.01
F4-G	None	0.00	100.0 \pm 0.1	46.0 \pm 0.3	0.19 \pm 0.01

TABLE 6: Cake appearance of the freeze-dried NPs. The bulk NPs solutions were freeze-dried with various cryoprotectants at 0.25% (wt/v). The freeze-dried cakes were then identified as the following: intact with the same volume (IS), collapsed (C), and partially collapsed (PC).

Cryoprotectants	Formulations							
	Cake appearance							
	Tween 80		Tween 20		PVA		None	
0.1%	0.05%	0.1%	0.05%	0.1%	0.05%	0.1%	0.05%	
Sucrose	IS	PC	IS	IS	IS	IS	IS	IS
Glucose	PC	PC	IS	PC	IS	IS	IS	IS
Mannitol	PC	IS	IS	IS	IS	IS	IS	IS
Glycine	PC	IS	PC	IS	IS	IS	IS	IS
Glycerol	C	C	C	C	PC	PC	PC	PC
Dextran 40000	IS	IS	IS	IS	IS	IS	IS	IS
None	PC	PC	PC	IS	IS	IS	IS	PC

TABLE 7: Ease of reconstitution of the freeze-dried NPs. The freeze-dried cakes were reconstituted in the same volume of water and were given a score as the following: reconstituted immediately (++++), reconstituted after several manual inversions for 1 min (+++), reconstituted after vortex for 1 min (++) , reconstituted after sonication (+), and not reconstituted after sonication (0).

Cryoprotectant	Formulations							
	Ease of reconstitution							
	Tween 80		Tween 20		PVA		None	
0.1%	0.05%	0.1%	0.05%	0.1%	0.05%	0.1%	0.05%	
Sucrose	++	+	++	++	+	+	0	0
Glucose	++	++	++	+++	+++	+++	0	0
Mannitol	0	0	0	0	0	0	0	0
Glycine	0	0	0	0	0	0	0	0
Glycerol	+++	++	+	+++	+++	+++	0	0
Dextran 40000	0	0	0	0	0	0	0	0
None	0	0	0	0	0	0	0	0

TABLE 8: Aqueous solubility of freeze-dried NPs. The freeze-dried cakes were reconstituted in the same volume of water, vortexed for 1 min, and sonicated for 10 min, the insoluble material was removed by centrifugation, and the concentration of the total xanthenes in the supernatant was measured by UV spectrophotometry. The results are presented as average solubility ($\mu\text{g/mL}$).

Cryoprotectants	Formulations							
	Aqueous solubility ($\mu\text{g/mL}$)							
	Tween 80		Tween 20		PVA		None	
0.1%	0.05%	0.1%	0.05%	0.1%	0.05%	0.1%	0.05%	
Sucrose	714	83	429	46	460	305	144	
Glucose	786	566	371	457	198	482	236	
Mannitol	92	38	101	25	35	75	12	
Glycine	38	22	105	11	54	134	12	
Glycerol	1196	964	500	898	771	372	276	
Dextran 40000	54	104	309	27	28	148	26	
None	50	45	107	12	33	44	9	

The Relative Standard Deviation was $<0.4\%$ of the values presented in the table and was not included for simplicity purposes.

TABLE 9: Cryopreservation effect of glucose, glycerol, and sucrose. The bulk NPs solutions were freeze-dried with various concentrations of glucose, sucrose, and glycerol. The freeze-dried cakes were then reconstituted in the same volume of water, vortexed for 1 min, and sonicated for 10 min, the insoluble material was removed by centrifugation, and the concentration of the total xanthenes in the supernatant was measured by UV spectrophotometry. The results are presented as average solubility ($\mu\text{g/mL}$).

Cryoprotectant concentration % (wt/v)	Aqueous solubility ($\mu\text{g/mL}$)		
	Glucose	Sucrose	Glycerol
0.125	684.0 \pm 1.0	180.0 \pm 1.0	805.0 \pm 1.0
0.25	1013.0 \pm 1.0	545.0 \pm 1.0	1118.0 \pm 2.3
0.375	1245.0 \pm 1.0	1027.0 \pm 1.0	1153.0 \pm 1.0
0.5	1262.0 \pm 1.0	1228.0 \pm 1.0	947.0 \pm 1.0
0.75	1238.0 \pm 1.0	1259.0 \pm 1.5	993.0 \pm 1.0
1.0	1169.0 \pm 1.0	1180.0 \pm 5.4	1033.0 \pm 1.0

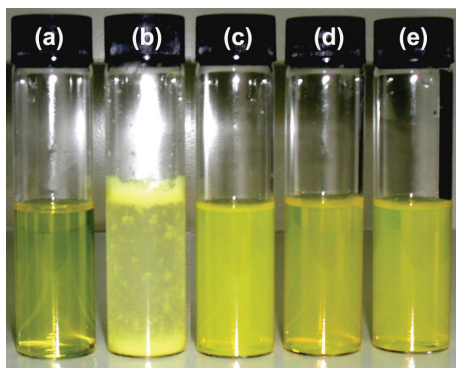


FIGURE 2: Appearance of the nanoparticle solutions. The NPs were prepared at polymer concentration of 50 mg/mL, 20% drug loading, and an aqueous phase of 0.1% tween 80. The NPs solution was photographed before freeze-drying (a) and after reconstitution of the freeze-dried NP cakes, without cryoprotectant (b), with 0.5% glucose (c), with 0.5% sucrose (d), and with 0.5% glycerol (e).

obtained with glucose and sucrose in the concentration range of 0.25–0.75% (wt/v).

Particle size measurements of the reconstituted NPs further confirmed the high cryopreservation efficiency of glucose and sucrose; the data indicate that particle size was slightly increased from 39 ± 0.1 nm to 43 ± 0.2 nm with 0.5% glucose and to 52 ± 0.2 nm with 0.5% sucrose. Furthermore, the percentage yield in these formulations was $100 \pm 1.0\%$.

3.9. Transmission and Scanning Electron Microscopy. TEM studies showed the presence of round NPs (Figure 3(a)), and studies in SEM showed the presence of spherical NPs (Figure 3(b)). The NPs freeze-dried without cryoprotectant showed irreversible agglomeration of NPs (Figure 3(c)), which explain their very low reconstitution. On the contrary, the NPs freeze-dried with glucose showed the presence of well-dispersed nanospheres embedded within a matrix of the cryoprotectant. This result indicates that glucose counteracts the freeze-drying stresses on NPs and hence hampers their agglomeration, maintains their integrity, and consequently eases their reconstitution. The SEM study may also give some insights into the presence of free extract in the NPs solution; the free compounds tend to crystallize upon freeze-drying, and the presence of crystals can be detected by SEM. However, SEM study of freeze-dried NPs showed the presence of nanospheres embedded within a matrix of the cryoprotectant and did not show the presence of any crystals. These results exclude the presence of free compounds in the NPs solution and further indicate that the high entrapment efficiency is due to entrapment of the compounds within the NPs.

3.10. Fourier Transform Infrared Spectroscopy. The intermolecular interaction between the drug and polymers commonly leads to changes in the FTIR patterns. FTIR pattern of the nonformulated xanthenes, E-RL100/E-RS100 mixture, loaded NPs, and the PMs of the xanthenes and polymers are

displayed in Figure 4. Matching up to FTIR spectrum of the xanthenes extract with the PMs at 20% drug concentration revealed no distinctive changes indicating that E-RL100/E-RS100 was not involved in intermolecular interaction with the xanthenes in the PMs. However, the intermolecular interaction between xanthenes and E-RL100/E-RS100 can be observed in the FTIR spectrum obtained for the loaded NPs (20% drug loading). The disappearance of the stretching of xanthenes hydroxyl (OH) at 3563, 3416, and 3251 cm^{-1} and the redshift in peak position of the polymer's carbonyl groups from 1723 to 1728 cm^{-1} may be attributed to the hydrogen bonding interaction between xanthenes OH groups and the Eudragit C=O groups in the loaded NPs. The hydrogen bonding between the compounds and the carriers may explain the high entrapment efficiency of the xanthenes in the Eudragit NPs.

3.11. In Vitro Release. Drug release was performed under sink conditions that guarantee solubility of released compounds, and the molecular weight cut-off of dialysis bags (8200 Da) allows diffusion of α -mangostin (410.5 Da) and γ -mangostin (396.4 Da) down their concentration gradient into the dialysis bags. However, α - and γ -mangostin could not be detected in the receiver compartment at the GIT-pH range after 48 h, and hence the cumulative release was 0%. Absence of drug release can be explained due to the strong interaction between the drug and the carrier molecules, which can be attributed to the number of hydrogen bonds between the xanthenes and the polymers (theoretically, 3 hydrogen bonds in α -mangostin and 4 in γ -mangostin). Similar results were reported in our previous study on α -mangostin/PVP solid dispersions, where the hydrogen bonding between α -mangostin and PVP prevented the release of α -mangostin in abiotic system, but the drug was released in the intracellular compartments of colon cancer cells [28]. The drug release result may also give insights into the presence of free compounds in the NPs solutions; the free compounds (if any) can diffuse through the dialysis membrane into the receiver compartment. Since the marker compounds were not detected in the receiver compartment, this excludes the presence of untrapped drug in the NPs solution. This result further supports our conclusion that the high drug entrapment efficiency is not due to presence of free drug.

3.12. Intracellular Delivery and Cytotoxicity on Colorectal Carcinoma Cells. Since there is no drug release in abiotic system, the drug release was then investigated in a biotic system made of HCT 116 colon cancer cells as a model cell line of colon cancer. The fluorescent properties of the xanthenes extract (excitation and emission wavelengths at 425 and 480 nm) were employed to investigate the cellular uptake of the NPs [28]. Cellular uptake of the cationic NPs was apparent after 6 h of treatment as evident by the presence of blue to green fluorescence in the cytoplasm of treated cells. On the other hand, untreated cells did not show any fluorescence and could hardly be seen (Figure 5). This result suggests that cellular uptake of the xanthenes-loaded NPs may be mediated via endocytosis, which is facilitated by electrostatic interaction between the cationic NPs and anionic cytoplasmic membrane

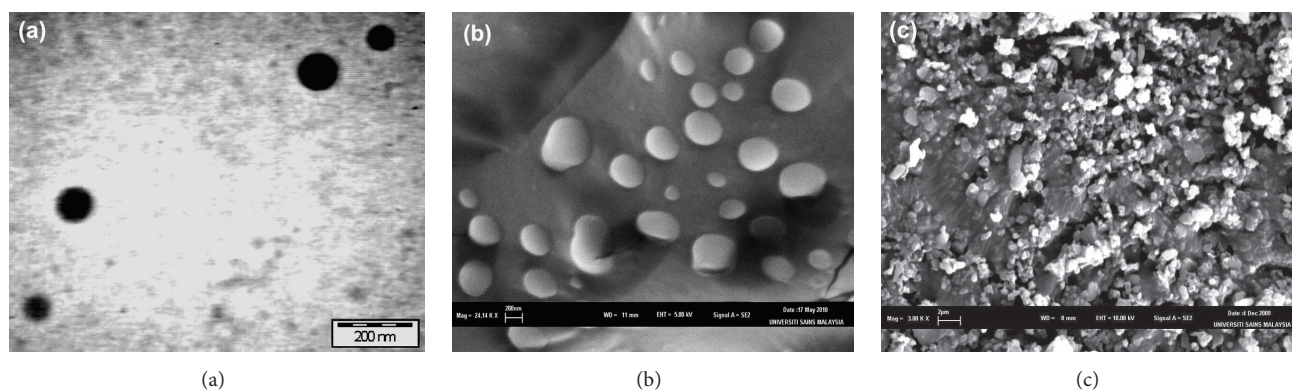


FIGURE 3: TEM and SEM micrographs of nanoparticles. The NPs prepared at 20% drug loading and aqueous phase of 0.1% tween 80 were studied by TEM (a). The same NP formulation was freeze-dried with and without cryoprotectant and was studied by SEM: micrograph of freeze-dried NPs with 0.5% glucose (b) and SEM micrograph of freeze-dried NPs without cryoprotectant (c).

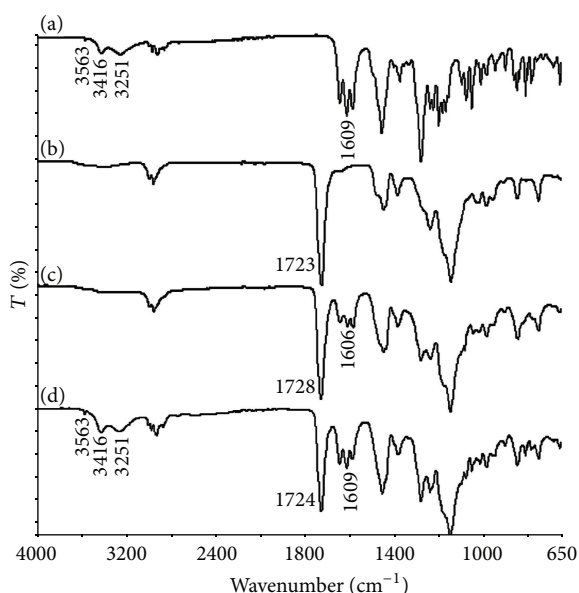


FIGURE 4: Fourier transform infrared spectroscopy. Free xanthenes extract (a), empty nanoparticles made of E-RL100:E-RS100 at 3:1 ratio (b), loaded nanoparticles at 20% drug loading (c), and physical mixtures at 20% drug concentration (d).

of HCT 116 cells. In our previous report, we showed endocytotic uptake of α -mangostin/PVP nanomicelles by HCT 116 colorectal carcinoma cells [28]. Other studies also reported endocytotic uptake of NPs in HCT 116 cells and other cancer cell lines [32, 33].

The cytotoxic effect was then investigated, which gave indirect insights into the intracellular drug release. Firstly, the morphology of cells was studied using the cytoplasmic shrinkage and loss of attachment as apoptotic markers. The results showed rapid changes, within <6 h, in cells treated with the free extract. On the other hand, cells treated with the loaded NPs required >24 h to start showing the same changes.

These results indicate delayed onset of cytotoxicity of the NPs, most likely due to the slow drug release. Secondly, the cytotoxic effect was measured quantitatively after incubating the cells for 48 h with the loaded and empty NPs. The results indicate the empty NPs (prepared under the same conditions but without the drug) were not cytotoxic to HCT 116 cells. On the contrary, the free xanthenes and xanthenes-loaded NPs caused a dose-dependent killing of cells (Figure 6); IC_{50} s were 6.6 ± 0.30 and 26.3 ± 0.22 $\mu\text{g}/\text{mL}$, respectively. It is noteworthy to point out that drug release was not detected in abiotic system under similar conditions of temperature, pH, and time of the cell culture medium, which, in conjunction with cellular uptake and cytotoxicity studies, further supports the conclusion of intracellular drug delivery and release.

Though cytotoxicity of the extract is reduced almost 4-fold in the NPs, the xanthenes solubility in the NPs is improved from 0.1 to 1250 $\mu\text{g}/\text{mL}$. In addition, the endocytotic uptake of NPs may increase the intracellular delivery of xanthenes and reduce the likelihood of developing drug resistance by cancer cells.

4. Conclusions

NPs of the xanthenes extract were produced at high entrapment efficiency and percentage yield in Eudragit RL100 and Eudragit RS100 by the nanoprecipitation method. Freeze-drying of the bulk NPs solutions allowed collection of the NPs at high percentage yield, which can be used as a new approach in the collection of NPs. The methodological simplicity and the reproducibility of procedures make the upscale production of NPs applicable by this method. The high entrapment efficiency can be attributed to the hydrogen bonding interaction between the xanthenes and the carrier molecules. The substantial enhancement of xanthenes solubility, the endocytotic uptake of the cationic NPs, and the intracellular delivery of xanthenes may provide a novel drug delivery system for the treatment and prevention of the gastrointestinal tract tumors, particularly tumors of the small intestine and the colon. In addition, the sustained

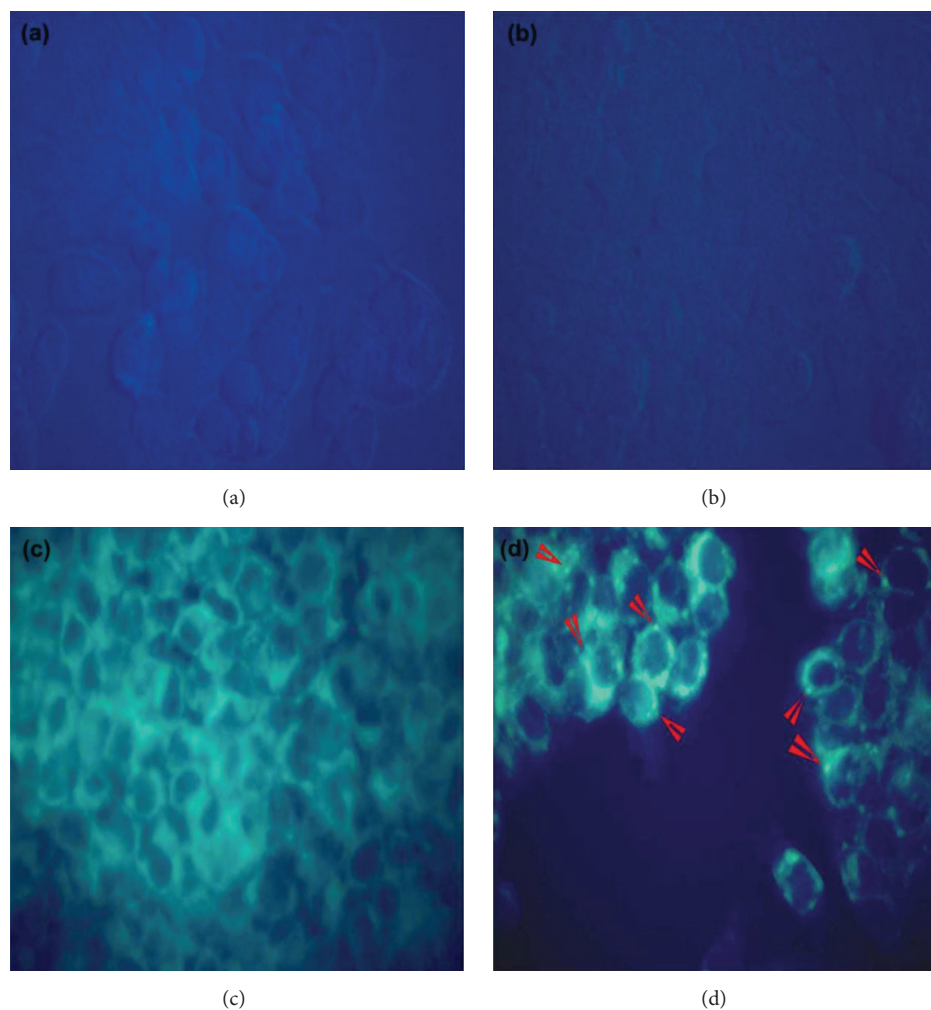


FIGURE 5: Cellular uptake of nanoparticles in colorectal carcinoma cells. HCT 116 cells were treated with the loaded NPs, empty NPs, or the vehicle (0.5% DMSO) for 6 h and photographed at 96x magnification under the blue filter of fluorescent microscopy. Cells treated with the vehicle (a), empty NPs (b), free extract (c), and loaded NPs (d).

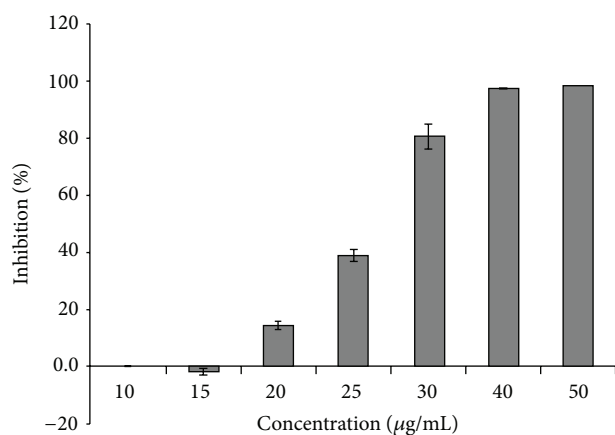


FIGURE 6: Dose response cytotoxicity of the loaded nanoparticles. HCT 116 human colorectal carcinoma cells were treated with loaded nanoparticles for 48 h, cell viability was determined by XTT test, and the results are shown as percentage inhibition relative to the negative control (0.5% DMSO).

intracellular release and the delayed onset of cytotoxicity may have advantages of reducing the dosing frequency and hence will be more convenient for patients. The NPs of the xanthenes can be produced for oral delivery such as in capsule form, or in suppositories for topical application via the rectal route for the treatment of rectal carcinomas. However, there is a need to study the *in vivo* anti-colon cancer activity, pharmacokinetics, and toxicity profile of these NPs.

Conflict of Interests

The authors declare that there is no conflict of interests regarding the publication of this paper.

Acknowledgments

This work was supported partially by the research chair of “Medical Applications of Nanomaterials” at King Saud University (KSU), Riyadh, Saudi Arabia. The work was also

partially supported by Universiti Sains Malaysia (USM) by providing a fellowship to the first author.

References

- [1] Y. Akao, Y. Nakagawa, M. Iinuma, and Y. Nozawa, "Anti-cancer effects of xanthenes from pericarps of mangosteen," *International Journal of Molecular Sciences*, vol. 9, no. 3, pp. 355–370, 2008.
- [2] J. Pedraza-Chaverri, N. Cárdenas-Rodríguez, M. Orozco-Ibarra, and J. M. Pérez-Rojas, "Medicinal properties of mangosteen (*Garcinia mangostana*)," *Food and Chemical Toxicology*, vol. 46, no. 10, pp. 3227–3239, 2008.
- [3] D. Obolskiy, I. Pischel, N. Siriwatanametanon, and M. Heinrich, "Garcinia mangostana L.: a phytochemical and pharmacological review," *Phytotherapy Research*, vol. 23, no. 8, pp. 1047–1065, 2009.
- [4] K. Matsumoto, Y. Akao, H. Yi et al., "Preferential target is mitochondria in alpha-mangostin-induced apoptosis in human leukemia HL60 cells," *Bioorganic and Medicinal Chemistry*, vol. 12, no. 22, pp. 5799–5806, 2004.
- [5] H. Doi, M.-A. Shibata, E. Shibata et al., "Panaxanthone isolated from pericarp of *Garcinia mangostana* L. suppresses tumor growth and metastasis of a mouse model of mammary cancer," *Anticancer Research*, vol. 29, no. 7, pp. 2485–2495, 2009.
- [6] S.-H. Hung, K.-H. Shen, C.-H. Wu, C.-L. Liu, and Y.-W. Shih, "α-mangostin suppresses PC-3 human prostate carcinoma cell metastasis by inhibiting matrix metalloproteinase-2/9 and urokinase-plasminogen expression through the JNK signaling pathway," *Journal of Agricultural and Food Chemistry*, vol. 57, no. 4, pp. 1291–1298, 2009.
- [7] J.-H. Yoo, K. Kang, E. H. Jho, Y.-W. Chin, J. Kim, and C. W. Nho, "α- and γ-Mangostin inhibit the proliferation of colon cancer cells via β-catenin gene regulation in Wnt/cGMP signalling," *Food Chemistry*, vol. 129, no. 4, pp. 1559–1566, 2011.
- [8] S. Tewtrakul, C. Wattanapiromsakul, and W. Mahabusarakam, "Effects of compounds from *Garcinia mangostana* on inflammatory mediators in RAW264.7 macrophage cells," *Journal of Ethnopharmacology*, vol. 121, no. 3, pp. 379–382, 2009.
- [9] L.-G. Chen, L.-L. Yang, and C.-C. Wang, "Anti-inflammatory activity of mangostins from *Garcinia mangostana*," *Food and Chemical Toxicology*, vol. 46, no. 2, pp. 688–693, 2008.
- [10] Y. Sakagami, M. Iinuma, K. G. N. P. Piyasena, and H. R. W. Dharmaratne, "Antibacterial activity of α-mangostin against vancomycin resistant *Enterococci* (VRE) and synergism with antibiotics," *Phytomedicine*, vol. 12, no. 3, pp. 203–208, 2005.
- [11] S. Suksamrarn, N. Suwannapoch, W. Phakhodee et al., "Antimycobacterial activity of prenylated xanthenes from the fruits of *Garcinia mangostana*," *Chemical and Pharmaceutical Bulletin*, vol. 51, no. 7, pp. 857–859, 2003.
- [12] P. D. Sampath and K. Vijayaraghavan, "Cardioprotective effect of α-mangostin, a xanthone derivative from *Mangosteen* on tissue defense system against isoproterenol-induced myocardial infarction in rats," *Journal of Biochemical and Molecular Toxicology*, vol. 21, no. 6, pp. 336–339, 2007.
- [13] J. Cui, W. Hu, Z. Cai et al., "New medicinal properties of mangostins: analgesic activity and pharmacological characterization of active ingredients from the fruit hull of *Garcinia mangostana* L.," *Pharmacology Biochemistry and Behavior*, vol. 95, no. 2, pp. 166–172, 2010.
- [14] H.-A. Jung, B.-N. Su, W. J. Keller, R. G. Mehta, and A. D. Kinghorn, "Antioxidant xanthenes from the pericarp of *Garcinia mangostana* (Mangosteen)," *Journal of Agricultural and Food Chemistry*, vol. 54, no. 6, pp. 2077–2082, 2006.
- [15] Y.-P. Tang, P.-G. Li, M. Kondo, H.-P. Ji, Y. Kou, and B. Ou, "Effect of a mangosteen dietary supplement on human immune function: a randomized, double-blind, placebo-controlled trial," *Journal of Medicinal Food*, vol. 12, no. 4, pp. 755–763, 2009.
- [16] L. Yu, M. Zhao, B. Yang, and W. Bai, "Immunomodulatory and anticancer activities of phenolics from *Garcinia mangostana* fruit pericarp," *Food Chemistry*, vol. 116, no. 4, pp. 969–973, 2009.
- [17] A. F. A. Aisha, K. M. Abu-Salah, Z. Ismail, and A. Majid, "In vitro and in vivo anti-colon cancer effects of *Garcinia mangostana* xanthenes extract," *BMC Complementary and Alternative Medicine*, vol. 12, article 104, 2012.
- [18] L. Li, I. Brunner, A.-R. Han et al., "Pharmacokinetics of alpha-mangostin in rats after intravenous and oral application," *Molecular Nutrition and Food Research*, vol. 55, supplement 1, pp. S67–S74, 2011.
- [19] N. Ubrich, C. Schmidt, R. Bodmeier, M. Hoffman, and P. Maincent, "Oral evaluation in rabbits of cyclosporin-loaded Eudragit RS or RL nanoparticles," *International Journal of Pharmaceutics*, vol. 288, no. 1, pp. 169–175, 2005.
- [20] A. Lopodota, A. Trapani, A. Cutrignelli et al., "The use of Eudragit RS 100/cyclodextrin nanoparticles for the transmucosal administration of glutathione," *European Journal of Pharmaceutics and Biopharmaceutics*, vol. 72, no. 3, pp. 509–520, 2009.
- [21] R. Pignatello, C. Bucolo, P. Ferrara, A. Maltese, A. Puleo, and G. Puglisi, "Eudragit RS100 nanosuspensions for the ophthalmic controlled delivery of ibuprofen," *European Journal of Pharmaceutical Sciences*, vol. 16, no. 1-2, pp. 53–61, 2002.
- [22] X. Dong, C. A. Mattingly, M. T. Tseng et al., "Doxorubicin and paclitaxel-loaded lipid-based nanoparticles overcome multidrug resistance by inhibiting P-glycoprotein and depleting ATP," *Cancer Research*, vol. 69, no. 9, pp. 3918–3926, 2009.
- [23] OECD, *OECD 105 Guidelines for the Testing of Chemicals, Water Solubility*, Organization for Economic Cooperation & Development, Paris, France, 1995.
- [24] H. Fessi, F. Puisieux, J. P. Devissaguet, N. Ammoury, and S. Benita, "Nanocapsule formation by interfacial polymer deposition following solvent displacement," *International Journal of Pharmaceutics*, vol. 55, no. 1, pp. R1–R4, 1989.
- [25] M. Sameti, G. Bohr, M. N. V. Ravi Kumar et al., "Stabilisation by freeze-drying of cationically modified silica nanoparticles for gene delivery," *International Journal of Pharmaceutics*, vol. 266, no. 1-2, pp. 51–60, 2003.
- [26] E. L. McConnell, H. M. Fadda, and A. W. Basit, "Gut instincts: explorations in intestinal physiology and drug delivery," *International Journal of Pharmaceutics*, vol. 364, no. 2, pp. 213–226, 2008.
- [27] A. Rajput, I. Dominguez San Martin, R. Rose et al., "Characterization of HCT116 human colon cancer cells in an orthotopic model," *Journal of Surgical Research*, vol. 147, no. 2, pp. 276–281, 2008.
- [28] A. F. A. Aisha, Z. Ismail, K. M. Abu-salah, and A. M. S. A. Majid, "Solid dispersions of α-mangostin improve its aqueous solubility through self-assembly of nanomicelles," *Journal of Pharmaceutical Sciences*, vol. 101, no. 2, pp. 815–825, 2012.

- [29] L. M. Jost, J. M. Kirkwood, and T. L. Whiteside, "Improved short- and long-term XTT-based colorimetric cellular cytotoxicity assay for melanoma and other tumor cells," *Journal of Immunological Methods*, vol. 147, no. 2, pp. 153–165, 1992.
- [30] U. Bilati, E. Allémann, and E. Doelker, "Development of a nanoprecipitation method intended for the entrapment of hydrophilic drugs into nanoparticles," *European Journal of Pharmaceutical Sciences*, vol. 24, no. 1, pp. 67–75, 2005.
- [31] S. De Chasteigner, G. Cavé, H. Fessi, J.-P. Devissaguet, and F. Puisieux, "Freeze-drying of itraconazole-loaded nanosphere suspensions: a feasibility study," *Drug Development Research*, vol. 38, no. 2, pp. 116–124, 1996.
- [32] H. Lee, C.-H. Ahn, and T. G. Park, "Poly[lactic-co-(glycolic acid)]-grafted hyaluronic acid copolymer micelle nanoparticles for target-specific delivery of doxorubicin," *Macromolecular Bioscience*, vol. 9, no. 4, pp. 336–342, 2009.
- [33] K. T. Thurn, H. Arora, T. Paunesku et al., "Endocytosis of titanium dioxide nanoparticles in prostate cancer PC-3M cells," *Nanomedicine: Nanotechnology, Biology, and Medicine*, vol. 7, no. 2, pp. 123–130, 2011.



Hindawi

Submit your manuscripts at
<http://www.hindawi.com>

